J. Earth Syst. Sci. (2022)131 123
https://doi.org/10.1007/s12040-022-01854-9

Geochronology and geochemistry of monzonitic granites from the eastern central Qilian Block, northwest China

Dongyi Lv[1], Erfeng Ren[1,*], Jilong Han[2], Binkai Li[3,4] and Sha Yang[1]

[1]*Department of Geological Engineering, Qinghai University, Xining 810 000, Qinghai, China.*
[2]*School of Chemical and Pharmaceutical Engineering, Hebei University of Science and Technology, Yuxiang Road, Shijiazhuang, People's Republic of China.*
[3]*Key Laboratory of Comprehensive and Highly Efficient Utilization of Salt Lake Resources, Qinghai Institute of Salt Lakes, Chinese Academy of Sciences, Xining 810 008, Qinghai Province, China.*
[4]*Qinghai Provincial Key Laboratory of Geology and Environment of Salt Lakes, Qinghai Institute of Salt Lakes, Chinese Academy of Sciences, Xining 810 008, Qinghai Province, China.*
**Corresponding author. e-mail: renerfeng998@163.com*

MS received 27 September 2020; revised 21 December 2021; accepted 22 December 2021

Eastern Central Qilian Block (E-CQB) is located in the Qilian orogenic belt, characterised by large outcrops of granite. The subduction age and geochemical processes of E-CQB are not precise. In this study, we conducted a comprehensive study of petrology, geochronology and whole-rock geochemistry of the Middle Ordovician granites (Sanlian rock mass) in the E-CQB. The results provide three key findings. First, the magmatic emplacement age of monzonite granites is about 466 Ma. Analysis derived from geochemical and geochronological revealed that the sample contains high-K, calc-alkaline, strongly peraluminous characteristics, and enriched in large-ion lithophile elements (LILEs; e.g., K, Th, and Rb). Depleting intensely in high field-strength element (HFSEs; e.g., Ti and P) then weakly in Nb, Ba, Sr and weak negative Eu. Monzonitic granites belong to S-type granites, can be divided into cordierite-bearing peraluminous granites, and the provenance is mainly partial melting of metapelite and metagreywacke. Second, combining the previous research and the new data obtained in this paper, the subduction age of E-CQB can be further refined to 444∼466 Ma.

Keywords. Geochronology; geochemistry; Qilian orogenic belt; Eastern Central Qilian Block; Middle Ordovician granites.

1. Introduction

The Qilian Orogenic Belt (QOB), one of the orogenic belt in the west of China, connects with the Inkling Orogenic Belt in the east and the Algin–West Kunlun Orogenic Belt in the west, forming the main part of the northern margin of the Qinghai–Tibet Plateau (Xiao *et al.* 2005; Yuan *et al.* 2005; Song *et al.* 2006; Zhang *et al.* 2006; Dong *et al.* 2007). The QOB records a long history of continental break up, seafloor spreading, and final continental collision from the Neoproterozoic to the Paleozoic (Li *et al.* 2017a, b; Liu *et al.* 2019; Song *et al.* 2009, 2014, Song and Niu 2013; Yang *et al.* 2015; Tung *et al.* 2016; Wang *et al.* 2016). Based on tectonics (Song *et al.* 2006, 2013, 2014), the QOB is divided into three sub-geotectonic units as following: (i) North Qilian Orogenic Belt

Published online: 24 May 2022

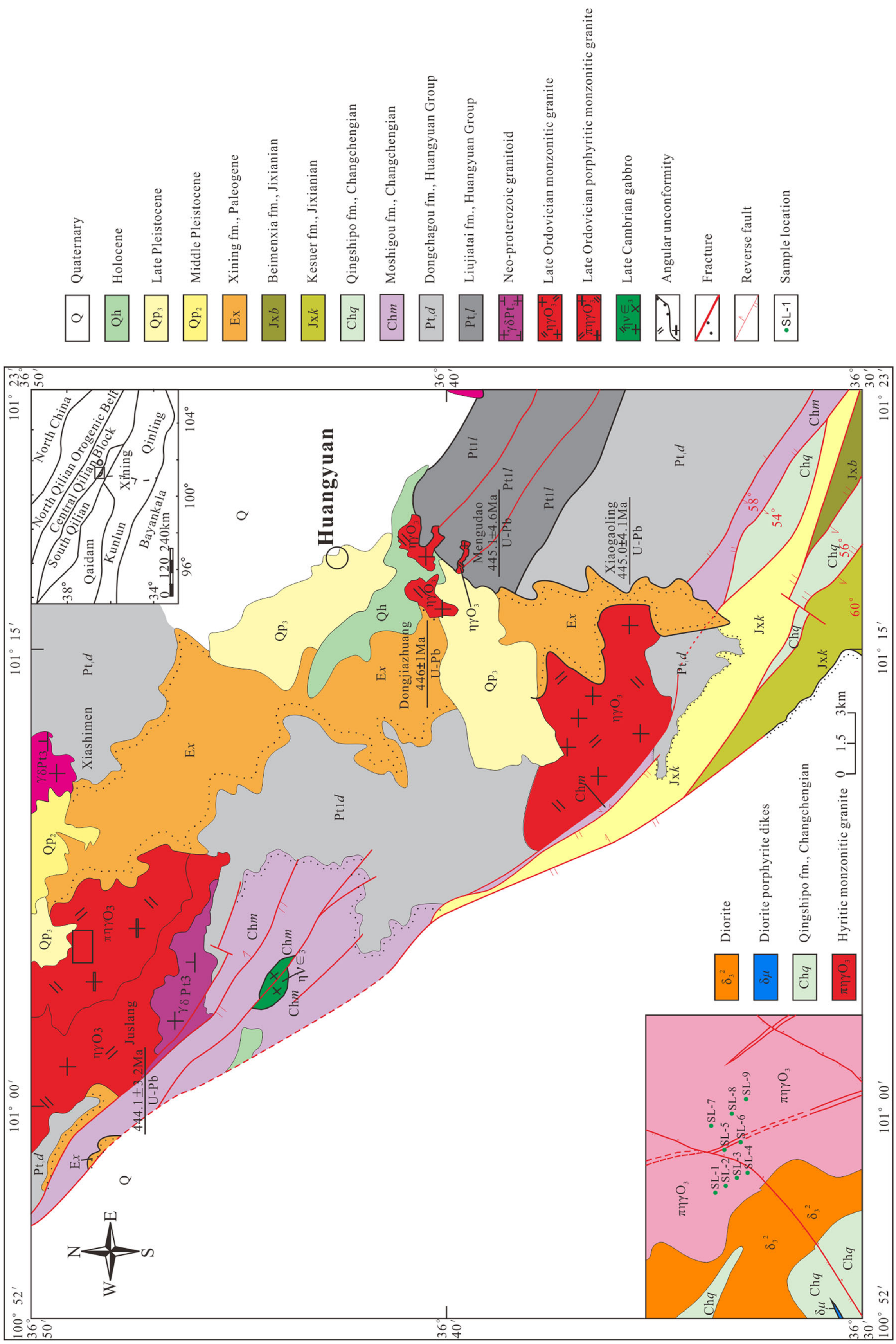

Figure 1. Simplified geological map of the Huangyuan area and the eastern QB, showing the sample locations. Modified after IGSQP.

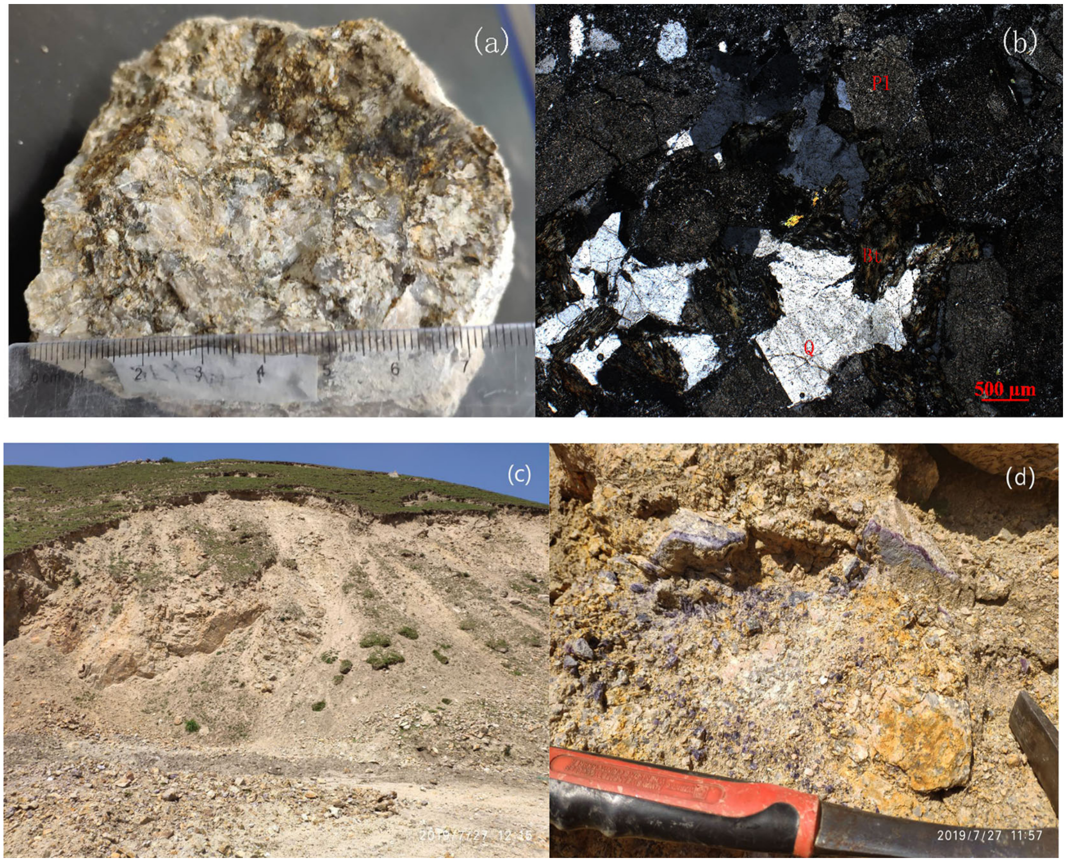

Figure 2. Hand specimen photographs and optical photomicrographs in cross-polarized light of the monzonitic granites from the Huangyuan area, E-CQB. **(a)** Hand specimen of monzonitic granite; **(b)** photomicrographs of monzonitic granite. Pl: plagioclase; Bt: biotite; Q: quartz; **(c)** field of monzonitic granites; **(d)** outcrop of monzonitic granites.

(NQ–OB), (ii) Central Qilian Block (CQB), and (iii) South Qilian Miogeosyncline Belt (SQ–MB) (Feng 1997; IGMGM 1965). The previous studies of QOB mainly focused on the Northern Qilian Orogenic Belt in the north and the Northern Qaidam Basin in the south. However, the study on the intermediate-acid intrusive rocks in the eastern section of Central Qilian Block (E-CQB) is relatively weak (Gao *et al.* 2017). Yong *et al.* (2008) proposed that there were two magmatic periods in the E-CQB and determined the ages of Dongjiazhuang rock mass with 446 ± 1 Ma and Xindian rock mass with 454 ± 5 Ma, respectively. Li *et al.* (2014) concluded that the Caledonian granite in the E-CQB was probably the result of mixed fusion of residual subducted oceanic crust and continental sediments, and determined the weighted average ages of two samples of Qingchengshan rock mass with 430.0 ± 4.1 and 420.2 ± 2.4 Ma, as well as the emplacement ages at 440.5 ± 2.5 Ma in Tongwei area. Then it was found that the weighted mean value of the surface age of $^{206}Pb/^{238}U$ of rock mass in Juslang; Mengundao and Xiaogaoling was 444.1 ± 3.2, 445.1 ± 4.6 and 445.0 ± 4.1 Ma, respectively (IGSQP 2015).

This study focused on the detailed geochronology and whole-rock geochemistry of granites from the Huangyuan area in the E–CQB, and discussed the petrogenesis and geological significance of these granites.

2. Geological setting and samples

The study area is located in the Sanlian area of Haiyan county, belonging to CQB of Caledonian fold system, adjacent to the NQ–OB in the north and the SQ–MB with the fault of the southern margin of the Central Qilian and the Qinghai–Gulei fault in the south (IGSQP 2015; figure 1).

The outcrop in the study area is relatively complete, including Dongchagou formation of Huangyuan Group (Pt_1d), Liujiatai formation of Huangyuan Group (Pt_1l), and Qingshipo formation of Changchengian (Chq). Lithologic assemblages of Dongchagou are mainly composed of

Table 1. *Major element compositions for the Sanlian monzonitic granitic.*

Sample	SL-1	SL-2	SL-3	SL-4	SL-5	SL-6	SL-7	SL-8	SL-9	SL-9R
SiO_2	75.92	71.59	71.75	72.21	71.13	72.98	72.87	70.34	73.45	73.53
TiO_2	0.19	0.29	0.31	0.22	0.24	0.24	0.31	0.39	0.32	0.33
Al_2O_3	12.76	14.94	14.74	13.82	13.21	13.86	13.83	14.75	13.49	13.60
Fe_2O_3	1.43	2.18	2.25	1.68	1.77	1.70	2.51	3.13	2.30	2.32
MnO	0.02	0.04	0.04	0.02	0.03	0.02	0.03	0.06	0.05	0.05
MgO	0.26	0.70	0.63	0.39	0.51	0.44	0.53	0.83	0.70	0.70
CaO	0.40	0.83	0.65	1.49	2.85	0.42	0.67	2.02	0.66	0.66
Na_2O	2.41	2.86	2.80	2.90	2.70	2.75	3.39	3.64	2.66	2.68
K_2O	4.78	4.70	4.95	5.27	4.87	5.28	4.20	3.14	3.31	3.32
P_2O_5	0.08	0.11	0.12	0.09	0.10	0.09	0.12	0.14	0.12	0.12
LOI	1.46	1.69	1.68	1.54	1.90	1.36	1.55	0.88	2.09	2.11
Total	99.71	99.93	99.92	99.63	99.31	99.15	100.00	99.33	99.15	99.41
σ	1.570	1.996	2.094	2.286	2.040	2.150	1.929	1.685	1.169	1.180
AR	3.406	2.838	3.034	3.290	2.786	3.568	3.196	2.360	2.457	2.454
SI	2.894	6.731	5.921	3.802	5.170	4.298	4.994	7.697	7.792	7.762
FL	94.707	90.048	92.289	84.576	72.636	95.005	91.850	77.102	90.033	90.073
MF	84.739	75.609	78.134	81.157	77.609	79.527	82.530	79.106	76.696	76.804
A/CNK	1.293	1.322	1.321	1.048	0.886	1.260	1.219	1.129	1.474	1.477
A/NK	1.397	1.527	1.477	1.319	1.359	1.354	1.366	1.570	1.696	1.699
R1	3041.36	2592.83	2559.46	2498.64	2587.30	2601.17	2595.29	2566.29	3107.75	3101.39
R2	550.12	692.84	663.23	711.19	836.08	599.75	627.83	815.00	617.24	621.57

Note: Samples with 'R' at the end of the sample number are parallel samples.

mica quartz schist, quartz mica schist, and phyllite with laminated marble, and Liujiatai is mainly composed of biotite plagioclase gneiss, biotite monzonitic gneiss, and plagioclase hornblende schist, with Caledonian rocks (such as diorite and granodiorite) intruding into it. However, lithologic assemblages of Moshigou are mainly composed of ash black to off-white and fresh red block stratified quartzite, with phyllite at the top of some sections, quartz-conglomerate near the bottom, and mica quartz schist at the bottom. Similar to Moshigou, lithologic assemblages of Qingshipo are mainly composed of ash black to black phyllite, platy phyllite, phyllite slate, silty slate and silty metasandstone, with a small amount of mica schist at the bottom. The overlying strata are Xining formation (Ex) of Paleogene system (IGSQP 2015).

There is Syncline with NW–SE axis direction is developed in Liujiatai formation of Huangyuan Group ($Pt_1 l$), and the core lithology is quartz mica schist, the two limbs are biotite plagioclase gneiss. Due to the influence of late magmatic activity, the synclinal landform is not complete.

Under the influence of frequent magmatic activities, intrusive rocks are widely developed and distributed, but the exposed area is not large. The intrusive body is generally elliptic, which can be divided into granodiorite ($\gamma\delta O_3$) and monzonitic granite ($\eta\gamma O_3$). The fault structure is well developed in the region, which is mainly NW or NWW trending longitudinal fault and NE or NEE trending transverse fault (IGSQP 2015).

Monzonite granites, located in the E-CQB and distributed in NW–SE direction, are distributed on both sides of deep and large faults and along the axis of the fold. And fluorite outcrops were found in it. Samples (SL; figure 2a) of monzonite granite are taken from the Sanlian area in Huangyuan, located in the E-CQB (36°49′16″N, 101°00′02″E), The samples are characterized by fractured granitic structure and blocky structure, which are mainly composed of biotite, plagioclase, potassium feldspar, quartz and opaque metallic minerals occasionally. Under the influence of brittle tectonics, the rock is broken and cemented by late siliceous hydrothermal solution, and about 20% of the debris is visible. They are characterized by the strong clayzation of plagioclase and chloritization of biotite. The biotite was produced by brown scaly structure aggregation with a particle size of 0.05–1.51 mm, and mainly distributed in the interstice of large

Table 2. *Trace element compositions for the Sanlian monzonitic granitic.*

Sample	SL-1	SL-2	SL-3	SL-4	SL-5	SL-6	SL-7	SL-8	SL-9	SL-1R
Trace element										
Rb	192.24	210.50	214.07	243.03	198.23	197.83	189.77	175.65	168.64	197.97
Ba	610.52	702.72	708.31	795.06	729.31	940.17	631.55	485.15	484.24	617.42
Th	15.20	26.49	22.96	20.35	20.12	17.64	23.40	27.02	26.96	15.93
U	2.53	8.59	7.38	3.10	3.20	2.96	4.46	3.58	4.16	2.53
Ta	1.68	2.11	2.14	1.69	1.73	1.80	2.44	2.72	2.76	1.72
Nb	13.28	19.71	21.13	15.16	16.29	17.44	21.79	24.97	23.06	13.48
Sr	169.87	222.75	224.48	176.91	209.14	222.99	175.67	261.38	164.77	170.72
Zr	108.81	160.78	154.96	121.11	148.94	134.90	161.07	200.00	181.63	108.06
Hf	3.06	4.39	4.37	3.34	4.05	3.78	4.64	5.53	5.16	3.06
Ti	1085.45	1828.59	1909.00	1349.76	1496.09	1507.28	1891.29	2401.07	1992.38	1128.23
Y	8.58	22.35	20.60	18.62	23.08	12.84	21.66	23.96	25.26	8.54
REE										
La	30.93	50.93	48.95	47.96	42.89	34.93	47.68	49.01	48.28	31.91
Ce	62.14	97.73	94.13	90.04	81.58	67.46	91.37	94.50	90.37	63.92
Pr	6.06	10.68	10.23	9.89	9.09	7.17	10.15	10.50	10.37	6.25
Nd	20.45	38.47	36.82	35.57	32.94	24.78	36.89	37.82	38.30	21.16
Sm	3.48	6.59	6.29	5.96	5.85	4.55	6.43	6.77	6.80	3.57
Eu	0.58	0.88	0.97	0.98	0.94	0.85	0.93	0.90	0.78	0.58
Gd	2.47	4.97	4.78	4.50	4.58	3.46	4.93	5.36	5.32	2.57
Tb	0.35	0.73	0.70	0.61	0.68	0.49	0.73	0.80	0.79	0.35
Dy	1.80	4.06	3.87	3.31	3.88	2.64	4.06	4.52	4.53	1.79
Ho	0.33	0.77	0.72	0.62	0.74	0.47	0.77	0.84	0.88	0.32
Er	0.89	2.14	1.93	1.71	2.01	1.24	2.06	2.27	2.41	0.84
Tm	0.13	0.33	0.29	0.26	0.30	0.18	0.32	0.34	0.37	0.13
Yb	0.85	2.07	1.81	1.64	1.91	1.18	2.02	2.14	2.40	0.80
Lu	0.13	0.31	0.27	0.24	0.28	0.18	0.29	0.32	0.36	0.12
$\sum$REE	123.63	205.28	197.38	190.4	173.28	139.73	193.45	199.49	194.9	127.39
LREE	6.95	15.38	14.38	12.89	14.4	9.85	15.18	16.59	17.06	6.92
HREE	17.78	13.35	13.73	14.77	12.04	14.19	12.75	12.03	11.42	18.42
LREE/HREE	26.04	17.62	19.45	20.94	16.1	21.32	16.93	16.45	14.41	28.68
$(La/Yb)_N$	130.58	220.66	211.76	203.3	187.68	149.58	208.63	216.08	211.95	134.31
Sm/Nd	0.17	0.17	0.17	0.17	0.18	0.18	0.17	0.18	0.18	0.17
δEu	0.57	0.45	0.52	0.55	0.54	0.63	0.49	0.44	0.38	0.56
δCe	1.05	0.98	0.98	0.96	0.96	0.99	0.97	0.97	0.94	1.04

Note: Samples with 'R' at the end of the sample number are parallel samples.

particles of quartz, feldspar or wrapped inside the particles. Most of the particles developed clayzation with a content of about 8%. The plagioclase is idiomorphic to semi-idiomorphic plate columnar with a particle size of 0.11–3.25 mm. It has a strong clayzation, and its fine and dense agglomerated twin crystals can be vaguely seen. Some of the particles are contained in the potassium feldspar particles, or are produced as inlaid particles, with a content of about 26%. The potassium feldspar is semi-idiomorphic to heteromorphic plate columnar, mainly striated feldspar and orthoclase, with the largest particle size up to cm. Most of the particles are relatively complete, often containing a large number of idiomorphic plate columnar plagioclase, the content is about 30%. The quartz accounts for 35% of the sample content, is heteromorphic with particle size between the plagioclase and potassium feldspar, and exhibits slight brittle structural fracture and slight wavy extinction (figure 2b).

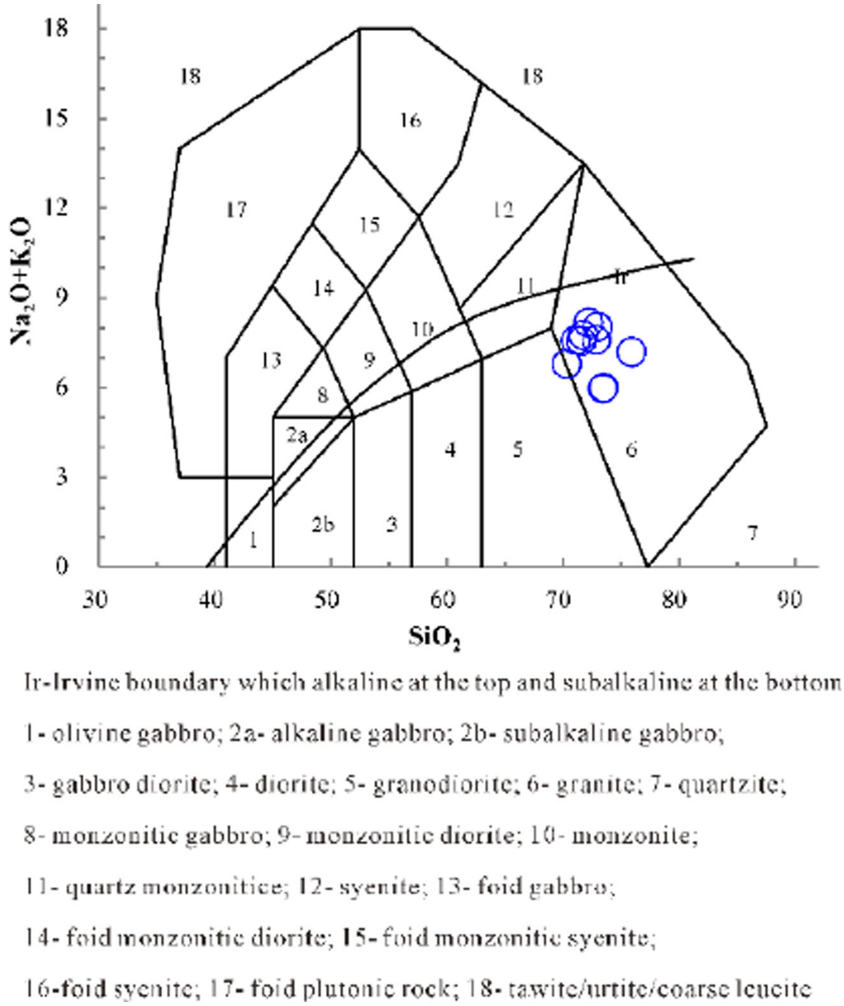

Figure 3. Classification diagram of principal elements of monzonitic granites from Huangyuan area.

The original rock is biotite monzogranite, which has a slight brittle tectonic fragmentation and forms about 20% detrital granite. Irregular metallic minerals can be seen occassionally, the content is about 1%.

3. Whole-rock geochemistry

Major element contents of the sample were determined by X-ray fluorescence (XRF) at the Beijing Kuangyan Geoanalysis Laboratory Co. Ltd. The analytical uncertainty is typically less than 5%. Trace element and rare earth element (REE) contents were determined using an Agilent 7500a inductively coupled plasma mass spectrometer (ICP-MS) at the Beijing Kuangyan Geoanalysis Laboratory Co. Ltd. (Liu *et al.* 2010). The detailed analytical procedures and precisions are the same as those described by Liu *et al.* (2008b). The major and trace element analytical results are listed in tables 1 and 2, respectively.

The sample chemistry was changed into a 'dry' system (excluding volatile water after converted to 100%), the main elements in the intrusive rock classification in the diagram (Middlemost 1985; figure 3), can be seen from the figure, granite rock sample points, nine points in the granite interval distribution, one point distribution within the range of granodiorite. The content of chemical composition of each intrusive rock is slightly different.

It can be seen from table 1 that the monzonitic granites have high contents of SiO_2 (70.34–5.92 wt.%), K_2O (3.14–5.28 wt.%), Na_2O (2.41–3.64 wt.%), and Al_2O_3 (12.76–14.94 wt.%). The samples showed calc-alkaline and high-K, calc-alkaline affinities on the SiO_2 *vs.* K_2O discrimination diagram (Peccerillo *et al.* 1976; figure 4a), calc-alkaline on AR *vs.* SiO_2 (Wrighe and Doherty 1970; figure 4b) and AFM plots (TFeO *vs.* Na_2O+K_2O *vs.* MgO,

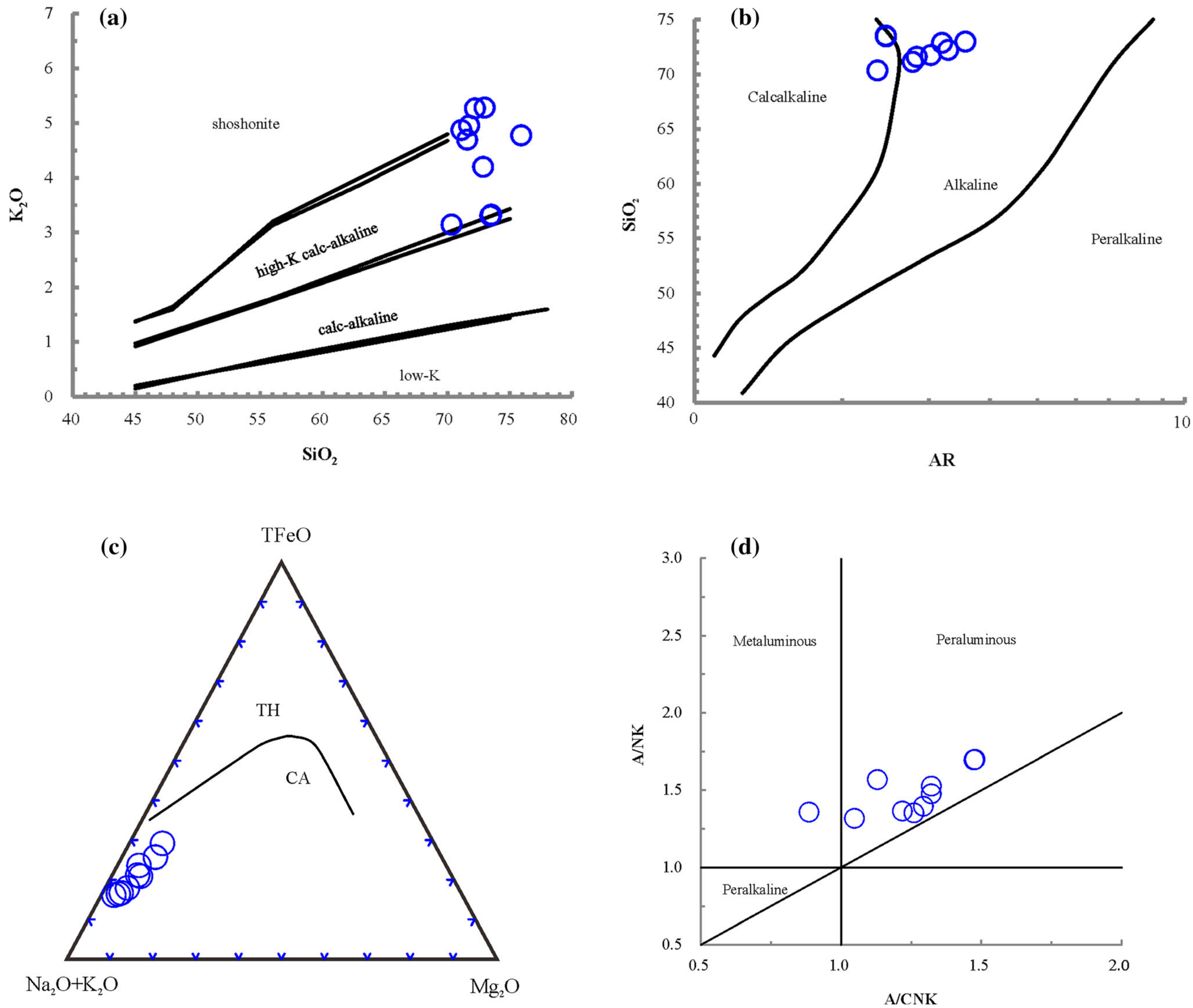

Figure 4. Discrimination diagrams of **(a)** SiO_2 *vs.* K_2O, **(b)** AR *vs.* SiO_2, **(c)** TFeO *vs.* (Na_2O+K_2O) *vs.* MgO and **(d)** A/CNK *vs.* A/NK showing compositions of the monzonitic granites from Huangyuan area. AR: alkalinity ratio, A: Al_2O_3, N: Na_2O, K: K_2O, C: CaO.

figure 4c) (Irvine and Baragar 1971) and strongly peraluminous compositions (0.886 < A/CNK < 1.477, 1.319 < A/NK < 1.699) on the A/CNK *vs.* A/NK discrimination diagram (Rickwood 1989; figure 4d). In addition, there are relatively low contents of MnO (0.02–0.06 wt.%), MgO (0.26–0.83 wt.%) and P_2O_5 (0.08 ~ 0.14 wt.%) in samples. Therefore, the monzogranite in the Huangyuan area is a peraluminous calc-alkaline rock.

Furthermore, the samples had $\sum$REE = 130.58–220.66 ppm with a slightly higher slope [$(La/Yb)_N$ = 14.41–28.68], which means that light rare earth elements (LREE) are enriched relative to heavy rare earth elements (HREE). Weak negative Eu anomalies with Eu/Eu* values of 0.38–0.63 (Rollinson 1983; figure 5a), which is shown that some plagioclase remained in the magma source area (unfinished plagioclase) or separated from the magma due to crystallization, resulting in granitic magma plagioclase loss (Sun and McDonough 1989).

In the spider diagrams, the nine samples show that they were clearly enriched in large-ion lithophile elements (LILEs; e.g., K, Th, and Rb), and strongly depleted in high field-strength element (HFSEs; e.g., Ti and P), weakly depleted in Nb, Ba and Sr (Sun and McDonough 1989, figure 5b). It is generally believed that the loss of Ti is caused by the crystallization of Ti-containing minerals, and the loss of P is caused by the crystalline differentiation of apatite, which

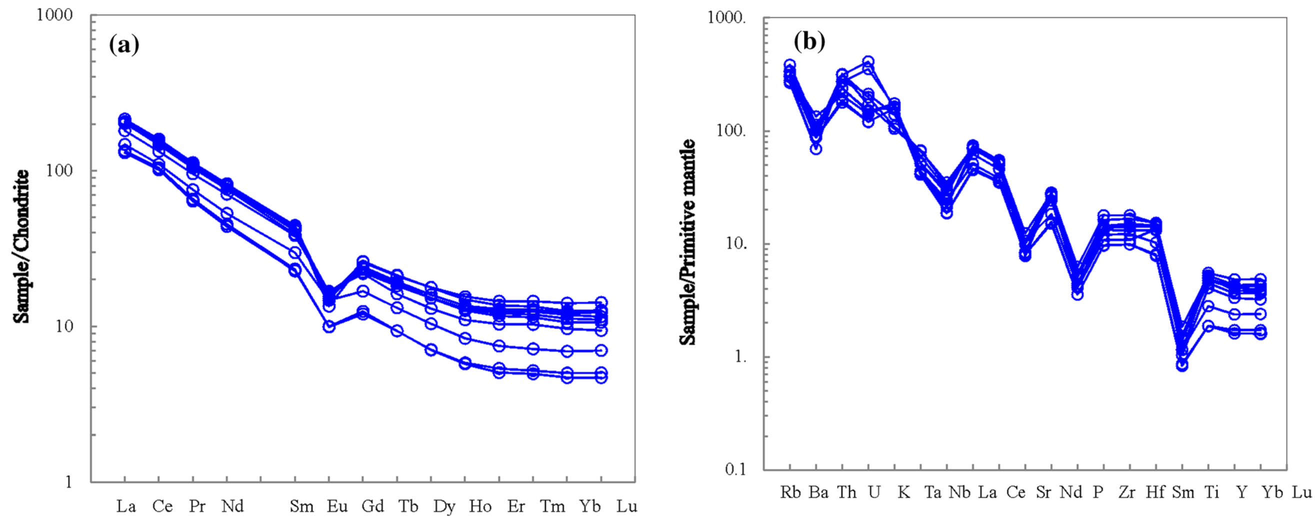

Figure 5. **(a)** Chondrite-normalized REE patterns and **(b)** primitive mantle-normalized spider diagrams of the monzonitic granites from Huangyuan area.

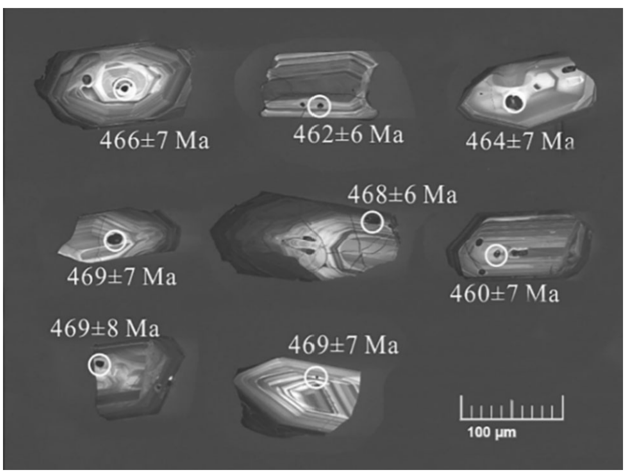

Figure 6. Representative CL images of zircons from samples SLCN.

indicates that they are derived from crust-derived magma or the magma was once crust-derived during the formation process.

4. Zircon U–Pb age analyses

Cathodoluminescence images (SL; figure 6) were acquired prior to U–Pb dating. Subsequently, zircon U–Pb dating was conducted using laser ablation inductively coupled plasma mass spectrometry (LA-ICP-MS) at the Beijing Kuangyan Geoanalysis Laboratory Co. Ltd. The detailed analytical procedures and precisions are the same as those described by Liu *et al.* (2008b). The off-line processing of the analysis data (including the selection of samples and blank signals, instrument sensitivity drift correction, element content and U–Th–Pb isotope ratio and age calculation) was completed by using the software ICPMSDataCal (Liu *et al.* 2008a, 2010).

Apart from a few dark browns, most Zircons from sample SLCN (Sanlian monzonitic granites) were predominantly colourless. And they had prismatic lengths ranging from 90 to 220 μm, aspect ratios of 2:1 to 3.5:1 (figure 6). Most of the zircons displayed a typical rhythmic oscillating zoning (often narrow zoning) in CL images, which could indicate a low-temperature magmatic origin (Pagel *et al.* 2000; Wu and Zheng 2004). Some zircons show signs of rounded edges, cones, and pits, suggesting that the zircons were subjected to later hydrothermal alteration or metamorphic processes.

The study focused on the above zircons with oscillating zonings. U–Pb isotope dating was carried out by LA-ICP-MS method and its isotope parameters were listed in table 3. The analysis revealed that the zircon Th/U ratio ranged from 1.07 to 2.18. On the U–Pb Concordia diagrams for zircons (figure 7a), the six analysis points give the older $^{206}Pb/^{238}U$ age (956–1356 Ma), which may be the inherited zircon age. In addition, there are two younger $^{206}Pb/^{238}U$ ages and two points deviating from the Concordia lines. Excluding the above analysis points, the $^{206}Pb/^{238}U$ ages of the remaining nine analysis points are all concentrated, with a weighted average of 466 ± 4.5 Ma (MSWD = 0.27; figure 7b). This age is the magmatic crystallization age of Huangyuan monzonitic granites.

Table 3. *LA-ICP-MS U–Pb data from zircons for the Sanlian monzonitic granites.*

Spot	U	Pb	Th	Th/U	$^{207}Pb/^{206}Pb$	1σ	$^{207}Pb/^{235}U$	1σ	$^{206}Pb/^{238}U$
SLCN-1	49095.6	147469.1	128567.5	1.15	0.0597	0.0024	0.6177	0.0281	0.0750
SLCN-2	355848.7	612157.8	528278.5	1.16	0.0716	0.0011	1.5866	0.0363	0.1605
SLCN-3	263803.9	1142531	578382.4	1.98	0.0597	0.0010	0.6122	0.0126	0.0742
SLCN-4	2191086	3613922	2291746	1.58	0.1980	0.0101	1.6513	0.0664	0.0634
SLCN-5	583513.7	2799327	1474562	1.90	0.0642	0.0015	0.6628	0.0170	0.0747
SLCN-6	103631.6	330228.5	241159.2	1.37	0.0573	0.0018	0.5975	0.0201	0.0755
SLCN-7	573513.8	1504351	1502216	1.00	0.0619	0.0011	0.6450	0.0149	0.0753
SLCN-8	474806.2	1282459	1444575	0.89	0.0562	0.0009	0.5548	0.0128	0.0714
SLCN-9	1.58E+10	2.76E+09	1E+09	2.75	0.9095	0.0111	29.3919	0.5243	0.2341
SLCN-10	1.47E+10	2.66E+09	9.73E+08	2.73	0.7987	0.0100	25.3429	0.3514	0.2297
SLCN-11	192519.6	636322	366483.6	1.74	0.0577	0.0026	0.5853	0.0254	0.0739
SLCN-12	423170.7	1273953	1018664	1.25	0.0610	0.0014	0.6373	0.0194	0.0754
SLCN-13	915342.3	3047472	1858000	1.64	0.0552	0.0011	0.6047	0.0140	0.0796
SLCN-14	1217448	1122985	1878596	0.60	0.0695	0.0010	1.5344	0.0340	0.1598
SLCN-15	571804.6	2160187	918392.3	2.35	0.0557	0.0016	0.5787	0.0173	0.0755
SLCN-16	319230.7	1128814	613042	1.84	0.0571	0.0020	0.5907	0.0231	0.0754
SLCN-17	2.97E+10	5.37E+09	1.89E+09	2.84	0.9070	0.0102	28.9986	0.4793	0.2317
SLCN-18	2.84E+10	5.26E+09	1.93E+09	2.72	0.7808	0.0100	24.7369	0.3367	0.2299

Spot	1σ	$^{208}Pb/^{232}Th$	$^{232}Th/^{238}U$	$^{207}Pb/^{206}Pb$	1σ	$^{207}Pb/^{235}U$	1σ	$^{206}Pb/^{238}U$	1σ
SLCN-1	0.0012	0.0193	1.0700	591	89	488	18	466	7
SLCN-2	0.0031	0.0276	0.9078	974	30	965	14	960	17
SLCN-3	0.0010	0.0150	1.5415	591	37	485	8	462	6
SLCN-4	0.0011	0.0465	1.0815	2810	84	990	25	396	7
SLCN-5	0.0011	0.0115	1.5378	750	49	516	10	464	7
SLCN-6	0.0011	0.0195	1.1985	502	69	476	13	469	7
SLCN-7	0.0010	0.0220	0.8017	672	39	505	9	468	6
SLCN-8	0.0012	0.0206	0.7448	461	31	448	8	445	7
SLCN-9	0.0036	0.4332	2.4082	–	–	3467	18	1356	19
SLCN-10	0.0022	0.4263	2.2246	–	–	3322	14	1333	12
SLCN-11	0.0011	0.0208	1.4033	520	100	468	16	460	7
SLCN-12	0.0013	0.0198	1.0345	639	48	501	12	469	8
SLCN-13	0.0012	0.0179	1.1169	420	46	480	9	494	7
SLCN-14	0.0028	0.0456	0.4923	915	28	944	14	956	16
SLCN-15	0.0011	0.0196	1.8978	443	65	464	11	469	7
SLCN-16	0.0015	0.0197	1.3295	498	78	471	15	468	9
SLCN-17	0.0032	0.4144	2.3926	–	–	3453	16	1344	17
SLCN-18	0.0022	0.4061	2.1774	–	–	3298	13	1334	12

5. Discussion

5.1 *Timing of granite emplacement*

Zircon grains from the gneissic granite sample SL had length/width ratios ranging from 2:1 to 3.5:1 and showed oscillatory zoning in CL images (figure 6). They also showed high Th/U ratios ranging from 1.07 to 2.18, indicating a magmatic origin. In addition, the $^{206}Pb/^{238}U$ ages of the remaining nine analysis points are similar, with a weighted average of 466 ± 4.5 Ma (figure 7b), which represents the crystallization age of Huangyuan monzonitic granites.

The main emplacement age of the rock samples is the Ordovician. In addition, it can also be found that a small number of samples may contain records of late magmatic activity (396 Ma). At the same time, there are 956–1356 Ma residual cores of inherited zircons in the rock mass, it can be found that there was magma activity during this period (IGSQP 2015). The rock emplacement age is Ordovician, but may also contain records of late magmatic events (396 Ma). At the same time, there are 956–1356 Ma residual cores of inherited zircons in the rock mass, we can also see from other literature that there was magma activity during this period.

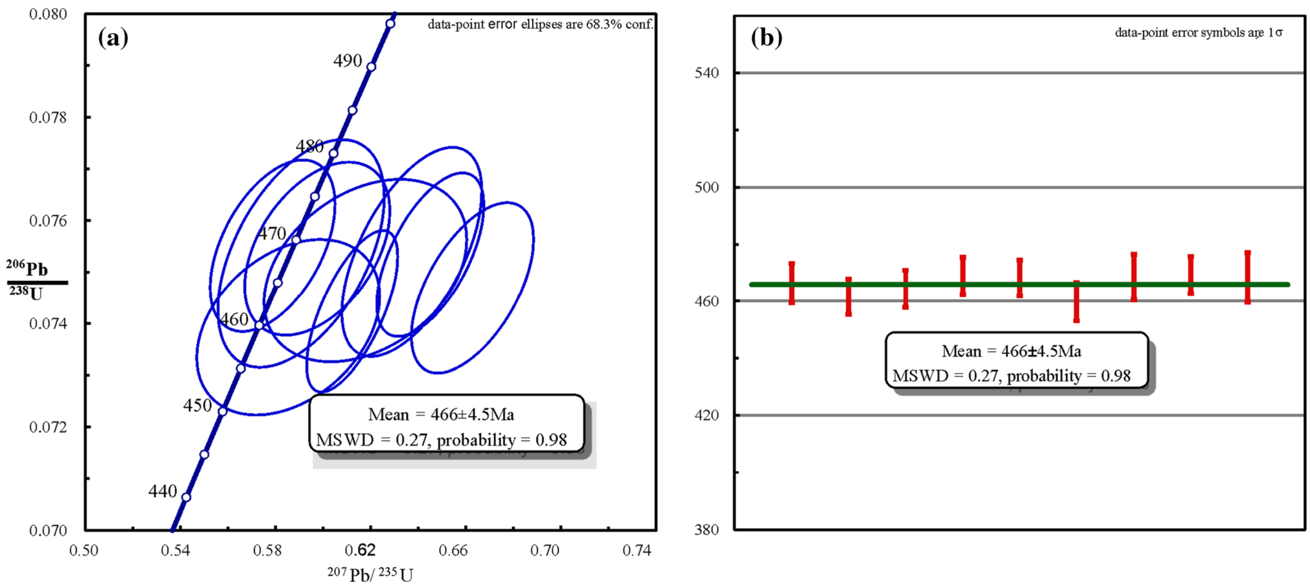

Figure 7. **(a)** U–Pb Concordia diagrams for zircons from the Huangyuan monzonitic granites and **(b)** their weighted average ages.

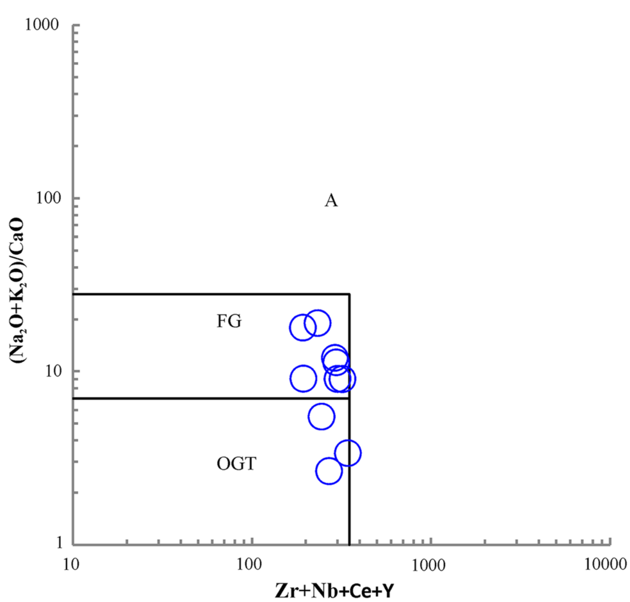

Figure 8. (Zr + Nb + Ce + Y) – (Na_2O + K_2O)/CaO classification diagram of monzonitic granites from the Huangyuan. FG: fractionated granite, OGT: other granite type.

5.2 *Petrogenesis and source nature*

The monzonitic granites in the study area have high contents of SiO_2 (70.34–75.92%), and the A/NK ratio (1.32–1.70) is greater than the average value of A-type granite (1.05). The TFeO/MgO value (1.41–2.52) is far less than the typical A-type granite (13.4), and it does not have the characteristics of A-type granite. Moreover, the Zr content (108.08×10^{-6} – 200.00×10^{-6}) and (Zr + Nb + Ce + Y) of Muscovite granite (192.80×10^{-6} – 363.43×10^{-6}) were significantly lower than that A-type granite (Zr > 250×10^{-6} and (Zr + Nb + Ce + Y)>350×10^{-6}). In the (Zr + Nb + Ce + Y) – (Na_2O + K_2O)/CaO classification diagram (Whalen *et al.* 1996; figure 8), Most of the samples fall into FG (fractionated granite) area and belong to the I-type, S-type and M-type granite with high fractionation. It is also clear that mica granite does not belong to A-type granite.

It is difficult or even impossible to identify I-type granite, S-type granite or A-type granite, since the mineral composition and chemical composition tend to be low co-coalescence granite when the above granites undergo highly fractionated crystallization (Chappell and White 1992; Chappell *et al.* 2000; Wu *et al.* 2007). Therefore, the identification of monzonitic granite needs to be discussed synthetically with petrographic and geochemical characteristics. In the Harker diagrams (figure 9), Al_2O_3, CaO, TFe_2O_3, MgO, TiO_2, and P_2O_5 contents in these granites decrease with increasing SiO_2. This geochemical signature of the monzonitic granites of Huangyan is characteristic of high-K, calc-alkaline, strongly peraluminous, and S-type granites.

The petrogenesis of peraluminous granites is usually attributed to be the result of Al-poor magma (Petford and Atherton 1996; Springer and Seck 1997; Sylvester 1998; Clemens 2003). The fractionation of Al-poor magma usually produces rocks containing metals, rich in Na, and low in

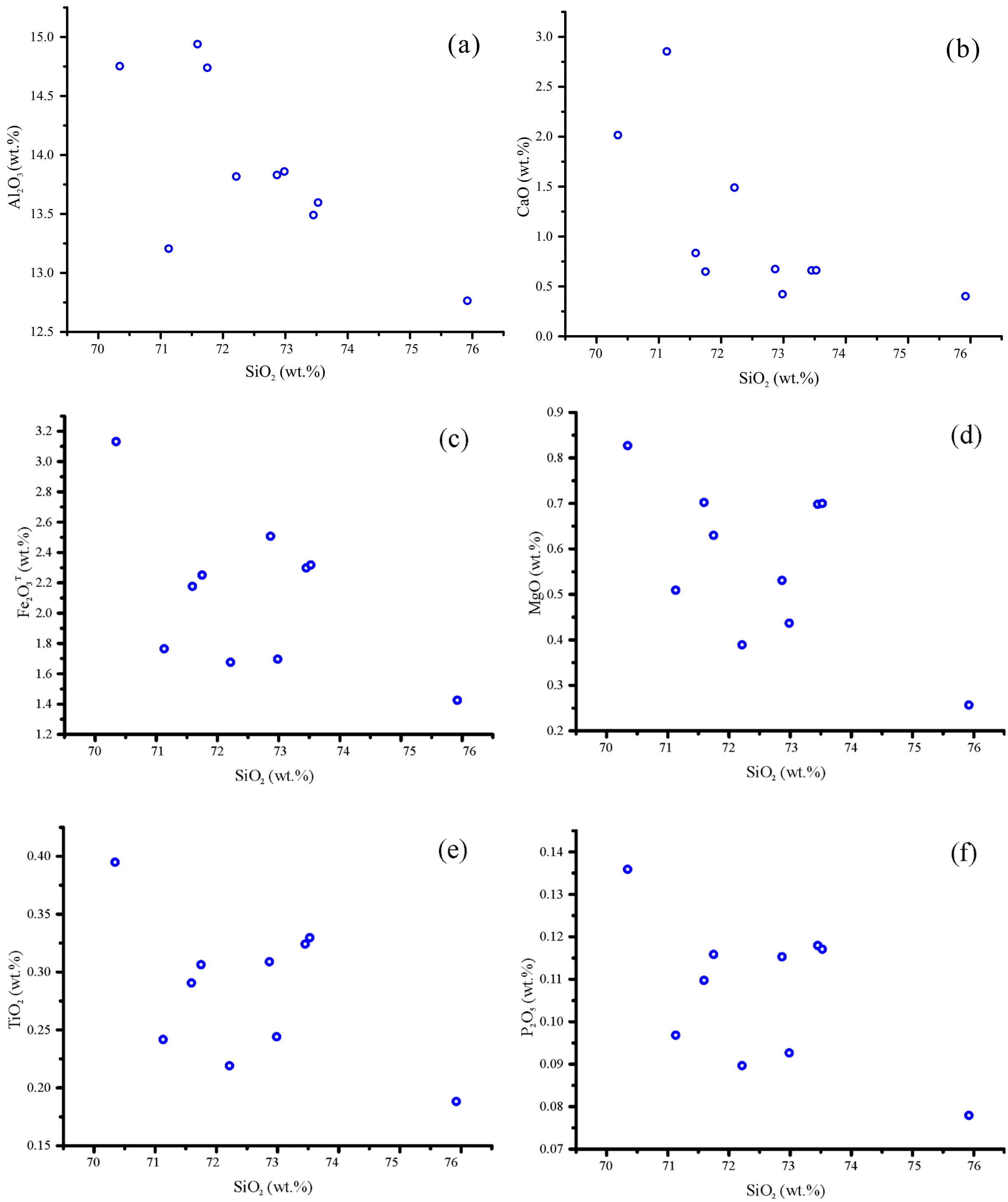

Figure 9. Harker diagrams illustrating major element variations in the monzonitic granites from the Huangyuan area.

K_2O/Na_2O acids in closed systems (Zen 1986; Gaudemer *et al.* 1988; Springer and Seck 1997; Sylvester 1998; Clemens 2003). However, the samples analyzed in the study are strongly peraluminous, K-rich rocks. Thus, the diagenesis of these granites cannot be explained simply by fractionation in a closed system (Liu *et al.* 2019). The finding is also supported by discrimination plots of Sm *vs.* La/Sm and La *vs.* $(La/Yb)_N$ (figure 10).

Previous researchers have proposed three origins of silica-rich, strong peraluminous granites: (1)

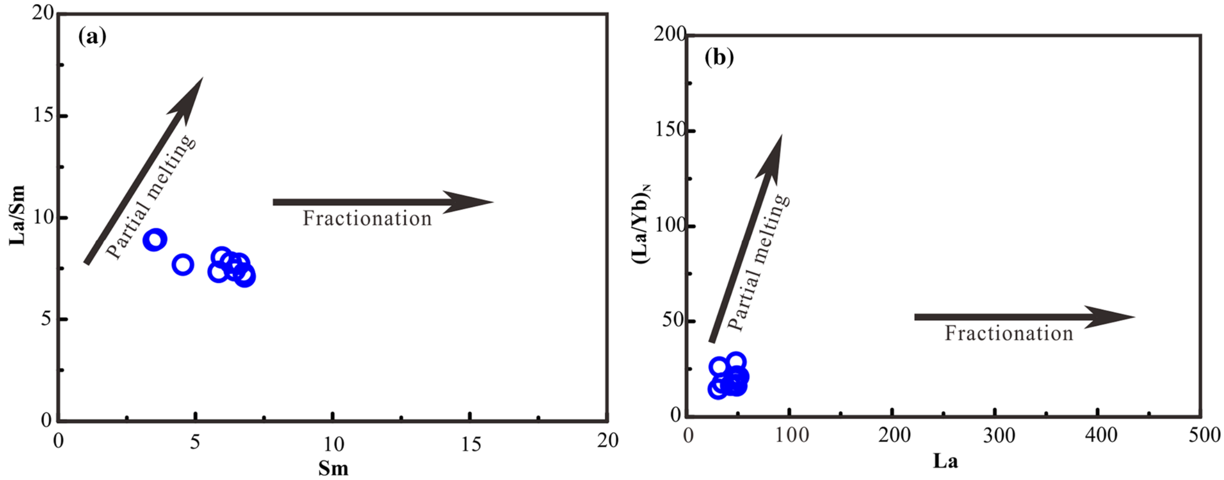

Figure 10. Compositional variation diagrams of **(a)** Sm *vs.* La/Sm and **(b)** La *vs.* $(La/Yb)_N$ for monzonitic granites from the Huangyuan area.

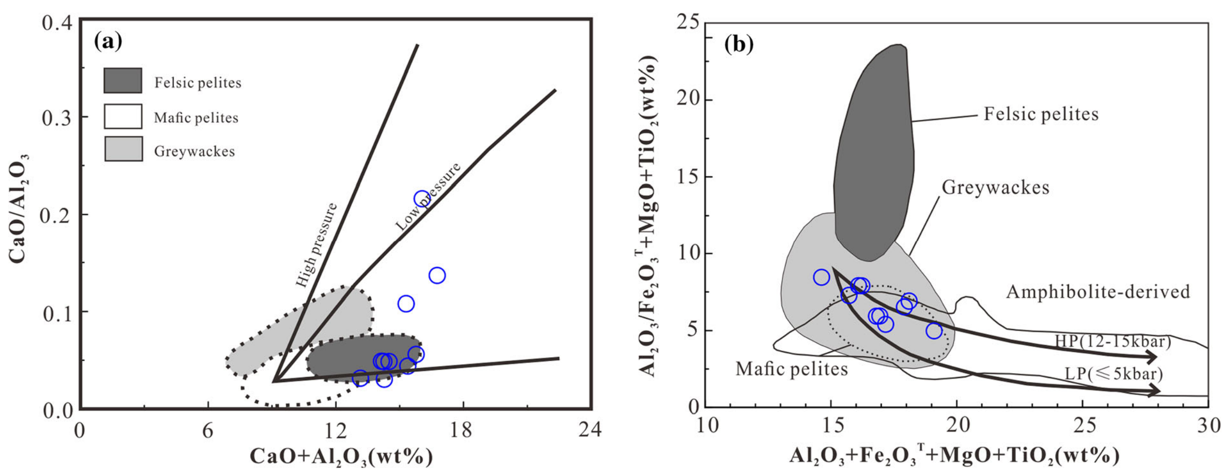

Figure 11. Diagrams of **(a)** $CaO + Al_2O_3$ *vs.* CaO/Al_2O_3; **(b)** $Al_2O_3 + Fe_2O_3^T + MgO + TiO_2$ *vs.* $Al_2O_3/(Fe_2O_3^T + MgO + TiO_2)$, for monzonitic granites from the Huangyuan area.

partial melting of Al-rich metapelite and metagreywacke (Miller 1985; Sylvester 1998; Patino Douce 1999); (2) tonalite and granodiorite at pressures ≥8 kbar with clinopyroxene in the restite (Patino Douce 1999); (3) partial melting of basaltic rocks and/or amphibolites under H_2O-saturated conditions (Ellis and Thompson 1986). The composition of most samples indicates that at low pressure (5 kbar $\leq P \leq$ 12 kbar, figure 11a, b), and the high K_2O/Na_2O ratios and negative Eu anomalies indicate a dominantly granitic melt generated under inconsistent H_2O-saturated conditions. Thus, most of the strongly peraluminous granites in our study may have been generated by partial melting of metapelite and metagreywacke, the others have been generated by tonalite and granodiorite.

The ratio of CaO/Na_2O (wt.%) can be used as an indicator of an S-type granite source, where melts produced from plagioclase-rich and clay-poor sources will tend to have higher ratios than melts derived from pelitic sources (Sylvester 1998). The gneissic granite samples show relatively lower CaO/Na_2O ratios (figure 12), suggesting that clay is the main source, and lower Al_2O_3/TiO_2 indicates that it was formed at high temperatures.

In A–B analysis (figure 13), the degree of aluminization decreases with the increase of the degree of differentiation of granite. In addition, it is considered that the mica minerals in granite are mainly biotite. The samples can be divided into cordierite-bearing peraluminous granitoids (CPGs) in the granitoid classification of Barbarin (1990) because of their strongly high aluminum content, and it must be the partial melting of sedimentary rock (Barbarin 1990, 1999). There is no cordierite in the granite, which may be due to the high water activity in the magma source area. In the

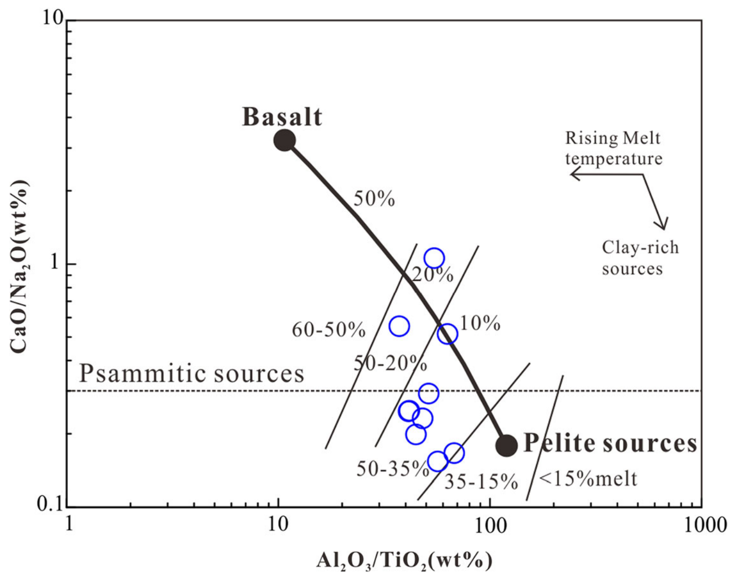

Figure 12. Diagrams of Al_2O_3/TiO_2 *vs.* CaO/Na_2O for monzonitic granites from the Huangyuan area.

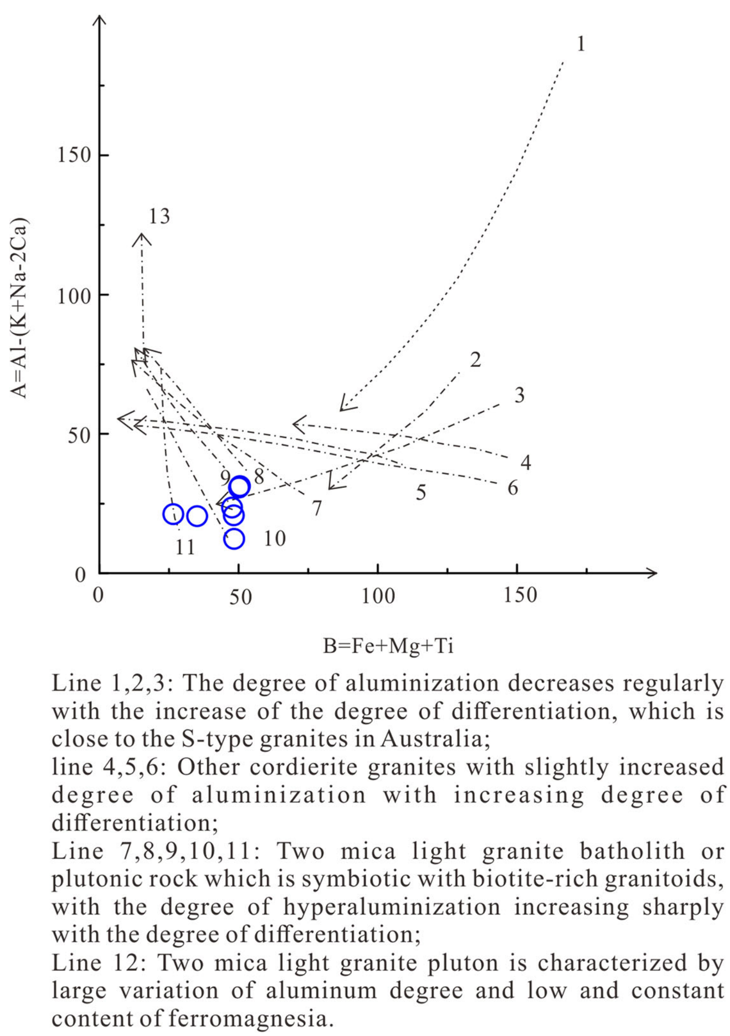

Figure 13. Diagrams of A *vs.* B for monzonitic granites from the Huangyuan area. A=Al–(K+Na+2Ca), reflecting the characteristics of Al. B=Fe+Mg+Ti decreased from most primitive granite magma to most evolved granitic magma.

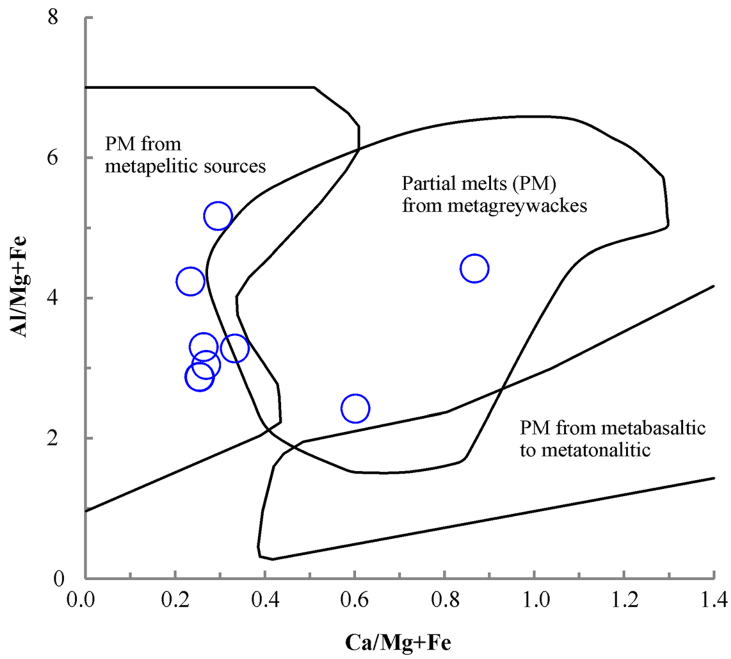

Figure 14. A/MF–C/FM classification diagram of monzonitic granites from the Huangyuan.

A/MF–C/FM classification diagram (Altherr *et al.* 2000; figure 14), almost all samples fall into the partial melts from metapelitic sources.

5.3 *Tectonic setting and implications*

Regarding the tectonic setting of the CQB in the Middle-Late Ordovician, many studies found that the granites were arc-type or collision-type granitoids (Wan *et al.* 2000, 2003; Gehrels *et al.* 2003; Liu *et al.* 2006; Chen *et al.* 2008; Tung *et al.* 2016). Previous studies suggested that CQB was formed at the active continental margin (Guo *et al.* 1999; Wan *et al.* 2000). Also, some basement rocks suggest an intraplate environment (Wan *et al.* 2000).

According to the geotectonic background of the study area and previous research data, the early Paleozoic evolution of the E-CQB can be roughly divided into four stages (Feng 1997; Xia *et al.* 1996): (1) Subduction of oceanic crust on both sides of Central Qilian in Late Cambrian to early Middle Ordovician; (2) the ancient ocean basin closed, and land (arc)–land collision occurred in middle–late of Middle Ordovician, the crust thickened during this period; (3) the subducting plate breaks off in Late Ordovician to late Early Silurian; (4) the crust melts under the influence of plate fragmentation in late Early Silurian to early Middle Silurian.

On the Y–Nb diagram of the granite (Pearce *et al.* 1984; figure 15a), the samples fall on the volcanic arc granite (VAG) area and the syn-collisional (Syn-COLG) area. Then, on the (Nb + Y)–Rb diagram of the granite (Pearce *et al.* 1984; figure 15b), the sample projection points are all located in the volcanic arc granite (VAG) region. Most of the samples on the R1–R2 diagram of the granite (Batchelor and Bowden 1985; figure 16a) fall on the area of pre-plate collisional granite, and several of the samples fall on mantle-differentiated granite.

In Rb/10-Hf-3Ta diagram of the granite (figure 16b), the samples are all located in the junction of WPG and collision of granite on the geotectonic background. In summary, the Middle Ordovician Huangyuan monzonitic granites (466 ± 4.5 Ma) are volcanic arc granite formed before the plate collision, and orogeny is about to happen.

The study area is adjacent to NQ–OB. According to the previous research, NQ–OB is a subduction zone, where subduction direction has some theories, such as northward subduction (Xu *et al.* 1994; Xia *et al.* 1995; Zhang and Xu 1997; Hou *et al.* 2005; Song *et al.* 2009), southward subduction (Wang and Liu 1976; Zuo and Wu 1997) and double subduction (Zuo and Wu 1987; Zuo and Liu 1997; Wu *et al.* 2006, 2011; Wang *et al.* 2008; Hou *et al.* 2015). Its subduction age is generally believed to have occurred at 469–445 Ma (Xia *et al.* 1996; Su *et al.* 2004).

According to the previous research, muscovite occurs in Dongjiazhuang rock mass (less than 5%), and R1–R2 discriminant maps of tectonic

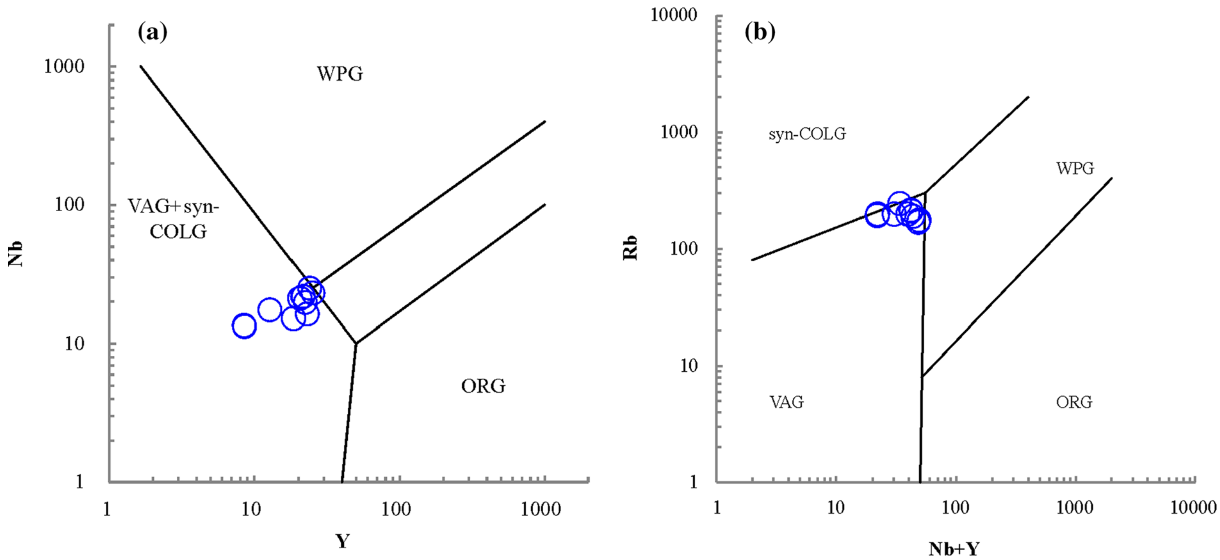

Figure 15. **(a)** Y–Nb classification diagram and **(b)** (Nb + Y)–Rb classification diagram of monzonitic granites from the Huangyuan area. WPG: Within-Plate Granite, ORG: Oceanic Ridge Granite, VAG: Volcanic Arc Granite, Syn-COLG: Syn-Collisional Granite.

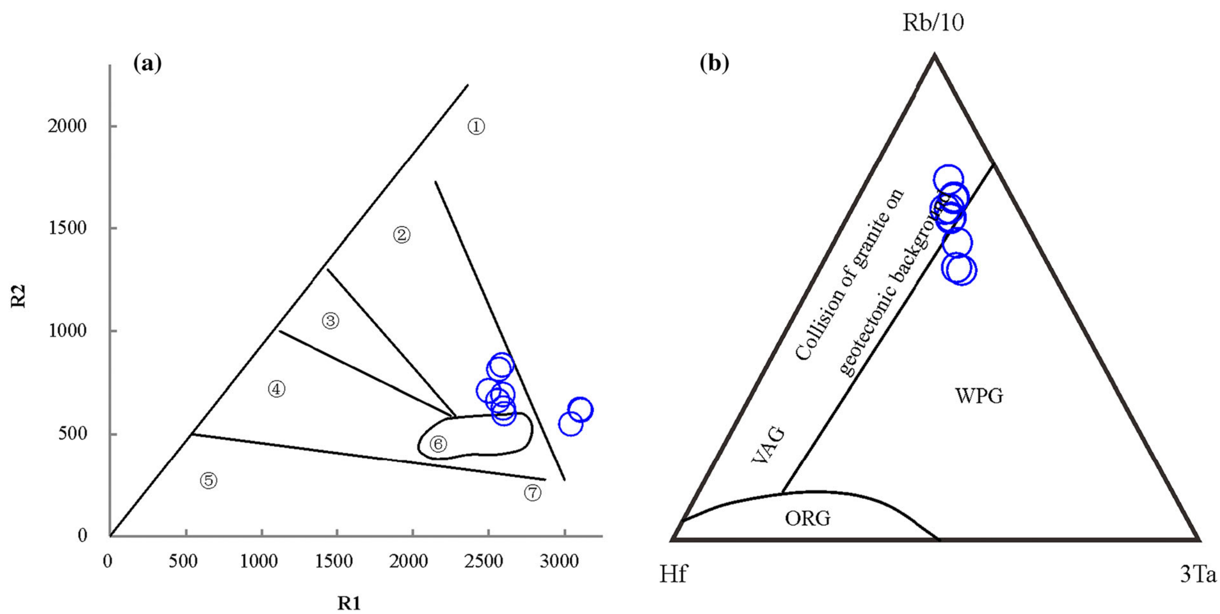

Figure 16. **(a)** R1–R2 classification diagram and **(b)** Rb/10–Hf–3Ta classification diagram of monzonitic granites from the Huangyuan area. ①: mantle-differentiated granite, ②: pre-plate collisional granite, ③: post-plate collisional granite, ④: late orogenic granite, ⑤: anorogenic granite, ⑥: syn-collisional granite, ⑦: post-orogenic granite, WPG: Within-Plate Granite, ORG: Oceanic Ridge Granite, VAG: Volcanic Arc Granite.

environment are concentrated in the collision zone (Yong *et al.* 2008). Therefore, the Middle Qilian was probably a Japanese-type island arc terrane in the early Paleozoic.

The late Ordovician Beigou rocks outcropped from the Lajishan belt in the south of the study area are similar to the standard Adakite and belong to the island arc (subduction) rock structural association (IAG). The discovery of Adakite further indicates that oceanic crust subduction occurred at that time. Adakites are closer to the trench than normal island-arc magmatic rocks (Defant and Drummond 1990). Therefore, the direction from Adakite to normal island-arc magmatic rocks represents the subduction direction of the oceanic crust.

The late Ordovician rocks, early diorites and granodiorites, continental arc (subduction) rock structural assemblages (CAG) occur in the Qilian belt. The occurrence of rocks in this period is the result of the closure of Lajishan small ocean basin and the subduction of ocean and continent, and the subduction of Lajishan small ocean basin can be further determined from the spatial position of the out-crowd intrusive rocks. The collisional granites exposed in late Ordovician and early Silurian belong to continental collisional rock tectonic assemblage (CCG). In the early late Ordovician, the lateral compression caused by subduction led to the shrinking of the residual basin, and in the late Ordovician, the basin closed and the collision of the middle and south Qilian continental blocks led to the formation of a new collisional orogenic belt. Therefore, the magmatic activity in the Qilian Mountains led to orogeny.

In the southeast direction of the study area, Dongjiazhuang rock (446 ± 1 Ma), Xindian rock (454 ± 5 Ma), Mengundao rock (445.1 ± 4.6 Ma) and Xiaogaoling rock (445.0 ± 4.1 Ma) (figure 1) belong to the contemporaneous rock mass. In other words, all are the Syn-COLG, Juslang rock (444.1 ± 3.2 Ma) belongs to anorogenic granite. But the samples from the study area were 466 ± 4.5 Ma which are pre-plate collisional granite. The comparison shows that the subduction age started at about 466 Ma, and ended at 444 Ma, which is early than previous research results.

6. Conclusions

By comparing the research results of this paper with those of previous studies, the following conclusions can be concluded:

(1) Monzonitic granites sampled in the Huangyuan area, E-CQB, formed at 466 ± 4.5 Ma. The geochemical and geochronological analyses of the samples show high-K, calc-alkaline, strongly peraluminous and S-type characteristics.
(2) The geochemical features of the samples indicate that the samples can be classified as cordierite-bearing peraluminous granitoids, and the provenance is mainly partial melting of metapelite and metagreywacke.
(3) The Middle Ordovician Huangyuan monzonitic granites are volcanic arc granite formed before the plate collision. The subduction age of E-CQB started at about 466 Ma and ended at 444 Ma.

Acknowledgements

The authors are grateful to the reviewers for their comments and suggestion. We thank Qipeng Yang and Xiaolong Zhu for providing help during lab experiments. This research was supported by Science and Technology project of Qinghai province (Grant Nos. 2018-ZJ-956Q) and 2019 Qinghai University two-level financial construction special project-key discipline construction project of geological resources and geological engineering (Grant No. 41250103).

Author statement

Dongyi Lv: Data curation, formal analysis, investigation, validation, writing original draft. Erfeng Ren: Methodology, visualization, writing – review and editing, fund acquisition. Jilong Han: Methodology, validation, writing – review and editing. Binkai Li: Conceptualization, supervision. Sha Yang: Material support.

References

Altherr R, Holl A, Hegner E, Langer C and Kreuzer H 2000 High-potassium, calc-alkaline I-type plutonism in the European Variscides: Northern Vosges (France) and northern Schwarzwald (Germany); *Lithos* **50** 51–73.

Barbarin B 1990 Granitoids: Main petrogenetic classifications in relation to origin and tectonic setting; *Geol. J.* **25** 227–238.

Barbarin B 1999 A review of the relationships between granitoid types, their origins and their geodynamic environments; *Lithos* **46** 605–626.

Batchelor R A and Bowden P 1985 Petrogenetic interpretation of granitoid rock series using multicationic parameters; *Chem. Geol.* **48** 43–55.

Chappell B W and White A J 1992 I- and S-type granites in the Lachlan Fold Belt; *Earth Environ. Sci. Trans. Roy. Soc. Edinburgh* **83** 1–26.

Chappell B W, White A J, Williams I S, Wyborn D and Wyborn L 2000 Lachlan Fold Belt granites revisited: Highland low-temperature granites and their implications; *J. Geol. Soc. Australia* **47** 123–138.

Chen J L, Xu X Y, Zeng Z X, Xiao L and Wang H L 2008 Geochemical characters and LA-ICPMS zircon U–Pb dating constraints on the petrogenesis and tectonic setting of the Shichuan intrusion, east segment of the Central Qilian, NW China; *Acta Petrol Sin.* **24** 841–854.

Clemens J D 2003 S-type granitic magmas-Petrogenetic issues, models and evidence; *Earth-Sci. Rev.* **61** 1–18.

Defant M J and Drummond M S 1990 Derivation of modem arc magmas by melting of young subducted lithosphere; *Nature* **347** 662–665.

Dong G A, Yang H R, Yang H Y, Liu D Y and Zeng J Y 2007 Zircon SHRIMP U–Pb geochronology of Precambrian basement and their geology implications in Qilian Block; *Chinese Sci. Bull.* **52** 1572–1585.

Ellis D J and Thompson A B 1986 Subsolidus and partial melting reactions in the quartz-excess $CaO+MgO+Al_2O_3+SiO_2+H_2O$ system under water-excess and water-deficient conditions to 10 kb: Some implications for the origin of peraluminous melts from mafic rocks; *J. Petrol.* **27** 91–121.

Feng Y M 1997 Investigatory summary of the Qilian Orogenic Belt, China: History, presence and prospect; *Adv. Earth Sci.* **12** 307–314.

Gao L, Ren E, Li J and Kang W H 2017 The geochemical characteristics and chronological significance of Baihuagou pluton at the eastern section of central Qilian; *J. Qinghai Univ.* **35** 1–7 (in Chinese).

Gaudemer Y, Jaupart C and Tapponnier P 1988 Thermal control on post-orogenic extension in collision belts; *Earth Planet Sci. Lett.* **89** 48–62.

Gehrels G E and Yin A and Wang X F 2003 Magmatic history of the northeastern Tibetan Plateau; *J. Geophys. Res.* **108**.

Guo J J, Zhao F Q and Li H K 1999 Jinningian collisional granite belt in the eastern sector of the Central Qilian Massif and its implication; *Acta Geosci. Sin.* **20** 10–15.

Hou K, Cheng Z, Hou R N, Wang J, Wang S and Xiang Z 2015 Geochemical characteristics and tectonic significance of the granotoids in the western section of the Mid-Qilian; *Adv. Earth Sci.* **30** 1034–1049.

Hou Q Y, Zhao Z D, Zhang H F, Zhang B R and Chen Y L 2005 Indian Ocean-MORB-type isotopic signature of Yushigou ophiolite in North Qilian Mountains and its implications; *Sci. China (Ser. D Earth Sci.)* **35** 710–719.

IGMGM 1965 The basic features of geotectonics in China; Industrial Press.

IGSQP 2015 Geological report of Liangji (J47E020020), Zhangzangsi (J47E020021), Huangyuan (J47E020022), Hudongzhongyangchang (J47E021020), Riyue (J47E02 1021), Tonghai (J47E021022), 1.50000; Industrial Press.

Irvine T N and Baragar W R A 1971 A guide to the chemical classification of the common volcanic rocks; *Can. J. Earth Sci.* **8** 523–548.

Li J L, Niu Y L, Chen S, Zhang Y, Sun W L and Liu Y 2014 Granite genesis in the Eastern Middle Qilian: Zircon U–Pb chronology, geochemistry and Sr–Nd–Hf isotopic evidence. *China Joint Conference on Earth Science.*

Li S, Zhao S, Liu X, Gao H, Yu S, Li X, Somerville I, Yu S and Suo Y 2017a Closure of the Proto-Tethys Ocean and Early Paleozoic amalgamation of microcontinental blocks in East Asia; *Earth Sci. Rev.* **186** 37–75.

Li S, Jahn B, Zhao S, Dai L, Li X, Suo L Guo L, Wang Y, Liu X, Lan H, Zhou Z, Zheng Q and Wang P 2017b Triassic southeastward subduction of North China Block to South China Block: Insights from new geological, geophysical and geochemical data; *Earth Sci. Rev.* **166** 270–285.

Liu Z W, Wang C L and Shi X H 2006 Granitoids characteristics and tectonic setting of Danghenanshan area in South Qilian Mountains; *Acta Geosci. Sin.* **20** 545–554.

Liu Y S, Hu Z C, Gao S, Xu J and Gao C G 2008a *In-situ* analysis of major and trace elements of anhydrous minerals by LA-ICP-MS without applying an internal standard; *Chem. Geol.* **257** 34–43.

Liu Y S, Zong K Q, Kelemen P B and Gao S 2008b Geochemistry and magmatic history of eclogites and ultramafic rocks from the Chinese continental scientific drill hole: Subduction and ultrahigh-pressure metamorphism of lower crustal cumulates; *Chem. Geol.* **247** 133–153.

Liu Y S, Gao S, Hu Z C, Gao C G, Zong K Q and Wang D B 2010 Continental and oceanic crust recycling-induced melt-peridotite interactions in the Trans-North China Orogen: U-Pb dating, Hf isotopes and trace elements in zircons from mantle xenoliths; *J. Petrol.* **51** 537–571.

Liu X T, Ren E F, Li B K, Du Y S, Gao D L, Ren Q H and Gao L 2019 Geochronology and petrogenesis of Neoproterozoic S-type granites from the Qilian Block, north-west China, and their geological implications; *Geol. J.* **54** 2364–2381.

Middlemost E A K 1985 *Magmas and Magmatic Rocks: An Introduction to Igneous Petrology;* Longman.

Miller C F 1985 Are strongly peraluminous magmas derived from pelitic sedimentary sources?; *J. Geol.* **93** 673–689.

Pagel M, Barbin V, Blanc P and Ohnenstetter D 2000 *Cathodoluminescence in Geosciences*; Springer, Germany.

Patino Douce A E 1999 What do experiments tell us about the relative contributions of crust and mantle to the origin of granitic magmas?; *Geol. Soc. London Spec. Publ.* **168** 55–75.

Pearce J A, Harris N B W and Tindle A G 1984 Trace element discrimination diagrams for the tectonic interpretation of granitic rocks; *J. Petrol.* **25** 956–983.

Peccerillo A and Taylor S R 1976 Geochemistry of Eocene Calc-alkaline volcanic rocks from the Kastamonu Area, Northern Turkey; *Contrib. Mineral. Petrol.* **58** 63–81.

Petford N and Atherton M 1996 Na-rich Partial melts from newly underplated basaltic crust: The Cordillera Blanca Batholith, Peru; *J. Petrol.* **37** 1491–1521.

Rickwood P C 1989 Boundary lines within petrologic diagrams which use oxides of major and minor elements; *Lithos* **22** 247–263.

Rollinson H R 1983 The geochemisrty of mafic and ultramafic rocks from the Archaean greenstone belts of Sierra Leone; *Mineral. Mag.* **47** 267–280.

Song S G, Zhang L F, Niu Y, Su L, Song B and Liu D Y 2006 Evolution from oceanic subduction to continental collision: A case study from the northern Tibetan Plateau based on geochemical and geochronological data; *J. Petrol.* **47** 435–455.

Song S G, Niu Y L, Zhang L F and Zhang G B 2009 Time constraints on orogenesis from oceanic subduction to continental subduction, collision, and exhumation: An example from North Qilian and North Qaidam HP-UHP belts; *J. Meteorol. Res.* **25** 2067–2077.

Song S G, Niu Y L, Su L, Zhang C and Zhang L F 2014 Continental orogenesis from ocean subduction, continent collision/subduction, to orogen collapse, and orogen recycling: The example of the North Qaidam UHPM belt, NW China; *Earth-Sci. Rev.* **129** 59–84.

Song S G, Niu Y L, Su L and Xia X 2013 Tectonics of the North Qilian orogen, NW China; *Gondwana Res.* **23** 1378–1401.

Springer W and Seck H A 1997 Partial fusion of basic granulites at 5 to 15 kbar: Implications for the origin of TTG magmas; *Contrib. Mineral. Petrol.* **127** 30–45.

Su J P, Hu N G, Zhang H F and Feng B Z 2004 U–Pb Zircon dating and genesis of the Heigouliangzi granitic intrusion in the western segment of the Middle Qilian Mountains; *Geoscience* **18** 70–74.

Sun S S and McDonough W F 1989 Chemical and isotopic systematics of oceanic basalts: Implications for mantle composition and processes; *Geol. Soc. London Spec. Publ.* **42** 313–345.

Sylvester P J 1998 Post-collisional strongly peraluminous granites; *Lithos* **45** 29–44.

Tung K, Yang H, Yang H, Liu D, Zhang J and Shau Y H 2016 Magma sources and petrogenesis of the early-middle Paleozoic backarc granitoids from the central part of the Qilian block, NW China; *Gondwana Res.* **38** 197–219.

Wan Y S, Yang J S, Xu Z Q and Wu C 2000 Geochemical characteristics of the Maxianshan Complex and Xinglongshan Group in the eastern segment of the Qilian Orogenic Belt; *J. Geol. Soc. China* **43** 52–68.

Wan Y S, Xu Z Q, Yang J S and Zhang J X 2003 The Precambrian high-grade basement of the Qilian Terrane and neighboring areas: Its ages and compositions; *Acta Geosci. Sin.* **24** 319–324.

Wang Q and Liu X Y 1976 Paleo-Oceanic crust of the Chilienshan region, western China and its tectonic significance; *Chinese J. Geol.* **11** 42–55.

Wang Y H, Jiao Y Q, Li J X and Lei G X 2008 Ordovician magmatic arc stratum of the middle Qilian block; *Geoscience* **22** 724–732.

Wang C, Li R S, Smithies R H, Li M and He S P 2016 Early Paleozoic felsic magmatic evolution of the western Central Qilian belt, Northwestern China, and constraints on convergent margin processes; *Gondwana Res.* **41** 301–324.

Whalen J B, Jenner G A, Longstaffe F J, Robert F and Gariépy C 1996 Geochemical and isotopic (O, Nd, Pb and Sr) constraints on A-type granite petrogenesis based on the Topsails Igneous Suite, Newfoundland Appalachians; *J. Petrol.* **37** 1463–1489.

Wrighe T L and Doherty P C 1970 A Linear programming and least squares computer method for solving petrologic mixing problems; *Geol. Soc. Am. Bull.* **81** 1995–2008.

Wu Y B and Zheng Y F 2004 Zircon genetic mineralogy and its constraints on U–Pb age interpretation; *Chinese Sci. Bull.* **49** 1589–1604.

Wu C L, Yao S, Yang J S, Zeng L S, Chen S Y, Li H B, Qi X X and Joseph L W 2006 Double subduction of the Early Paleozoic North Qilian oceanic plate: Evidence from granites in the central segment of North Qilian, NW China; *Geol. China* **33** 1197–1208.

Wu F Y, Li X H, Yang J H and Zheng Y F 2007 Discussions on the petrogenesis of granites; *Acta Petrol. Sin.* **23** 1217–1238.

Wu C L, Gao Y H, Frost B R, Robinson P T, Wooden J L, Wu S P, Chen Q L and Lei M 2011 An early Palaeozoic double-subduction model for the North Qilian oceanic plate: Evidence from zircon SHRIMP dating of granites; *Int. Geol. Rev.* **53** 157–181.

Xia L Q, Xia Z C and Xu X Y 1995 Dynamics of Tectono-volcano-magmatic evolution from North Qilian Mountains, China; *Northwest Geosci.* **16** 225–241.

Xia L Q, Xia Z C and Xu X Y 1996 *Petrogenesis of the Marine Volcanic Rocks from North Qilian*; Beijing: Geological Publishing House.

Xiao W J, Windley B F, Liu D Y, Jian P, Lui C Z, Yuan C and Sun M 2005 Accretionary tectonics of the Western Kunlun Orogen, China: A Paleozoic-Early Mesozoic, long-lived active continental margin with implications for the growth of Southern Eurasia; *J. Geol.* **113** 687–705.

Xu Z Q, Xu H F, Zhang J X, Li H B, Zhu Z Z and Qu J C 1994 The Zoulang Nanshan Caledonian Subduction Complex in the Northern Qilian Mountains and Its Dynamics; *Acta Geol. Sin.* **7** 225–241.

Yang H, Zhang H, Luo B, Zhang J, Xiong Z, Guo L and Pan F 2015 Early Paleozoic intrusive rocks from the eastern Qilian Orogen, NE Tibetan Plateau: Petrogenesis and tectonic significance; *Lithos* **224–225** 13–31.

Yong Y, Xiao W J, Yuan C, Zhen Y and Li J L 2008 Geochronology and geochemistry of Paleozoic granitic plutons from the eastern Central Qilian and their tectonic implications; *Acta Petrol. Sin.* **24** 855–866.

Yuan C, Sun M, Zhou M F, Xiao W and Hui Z 2005 Geochemistry and petrogenesis of the Yishak Volcanic Sequence, Kudi ophiolite, West Kunlun (NW China): Implications for the magmatic evolution in a subduction zone environment; *Contrib. Mineral. Petrol.* **150** 195–211.

Zen E A 1986 Aluminum enrichment in silicate melts by fractional crystallization: Some mineralogic and petrographic constraints; *J. Petrol.* **27** 1095–1117.

Zhang H F, Jin L L, Zhang L, Yuan H L and Zhang B R 2006 Pb and Nd isotopic compositions of basement and granitoid in the Qilianshan: Constraints on tectonic affinity; *Earth Sci.* **31** 57–65.

Zhang J X and Xu Z Q 1997 A tentative discussion on the ages of the subduction-accretionary complex/volcanic arcs in the middle sector of North Qilian Mountain; *Acta Petrol. Mineral.* **16** 112–119.

Zuo G C and Liu J C 1987 The evolution of Tectonic of Early Paleozoic in North Qilian Range, China; *Chinese J. Geol.* **17** 14–24.

Zuo G C and Wu H Q 1997 A bi-subduction-collision orogenic model of early-paleozoic in the middle part of North Qilian area; *Adv. Earthences* **12** 315–323.

Corresponding editor: Rajneesh Bhutani